New Control Strategies for Underactuated Tethered Formation Flight Spacecraft

Soon-Jo Chung*
Iowa State University, IA 50011, USA
Jean-Jacques E. Slotine,† and David W. Miller‡
Massachusetts Institute of Technology, MA 02139, USA

We introduce a decentralized attitude control strategy that can dramatically reduce the usage of propellant, by taking full advantage of the physical coupling of the tether. Motivated by a controllability analysis, indicating that both spin-up and relative attitudes are fully controllable by the reaction wheels, we report the first propellant-free underactuated linear and nonlinear control results for tethered formation flying spacecraft. We take a nonlinear control approach to underactuated tethered formation flying spacecraft, whose lack of full state feedback linearizability, along with their complex nonholonomic behavior, characterizes the difficult nonlinear control problem. We introduce several nonlinear control laws that are more efficient in tracking time-varying trajectories than linear control. We also extend our decentralized control approach to underactuated tethered systems, thereby eliminating the need for any inter-satellite communication.

I. Introduction

NASA's SPECS (Submillimeter Probe of the Evolution of Cosmic Structure) mission[7,9,11] is proposed as a Tethered Spacecraft Interferometer (TSI) that detects submillimeter-wavelength light from the early universe. The kinds of stellar objects that will be observed will contain information at many spatial frequencies, thus the ability of interferometers to observe at multiple baselines will be key. Tethered formation flight enables interferometric baseline changes with minimal fuel consumption; without tethers, a massive amount of fuel would be required to power the thrusters to change the baseline, as in the a Separated Spacecraft Interferometer (SSI) architecture.

Most of previous work on tethered satellites formation flight is based upon the assumption that the tethered system is fully actuated (both force F and torque u are available). Motivated by the controllability analysis, indicating that a planar rotating array of tethered spacecraft can control all relevant degrees of freedom using only one reaction wheel in each spacecraft, the aim of this paper is to introduce several new nonlinear control techniques for spinning tethered arrays without thrusters ($F = 0$). This article also fulfills the potential of the proposed strategy by providing a new momentum dumping method without the need for torque-generating thrusters; The compound pendulum mode and array spin rate are stabilized using only the linear thruster and translational actuator on the tether during the operation of momentum dumping.

Such a tethered system without thrusters is *underactuated* since it has fewer inputs than configuration variables. In contrast with linear systems in which an underactuated control law can be synthesized easily, designing a nonlinear controller for nonlinear underactuated systems poses a challenge, mainly due to lack of full state feedback linearizability. We exploit gain-scheduling linear control, feedback linearization via momentum decoupling, and backstepping. We shall consider only the case of the fixed tether length, focusing on the spin-up attitude control problem on the assumption that the tether length is controllable separately.

*Assistant Professor of Aerospace Engineering, AIAA Member, sjchung@alum.mit.edu.
†Professor of Mechanical Engineering & Information Sciences, Professor of Brain & Cognitive Sciences, jjs@mit.edu.
‡Professor, Department of Aeronautics and Astronautics, and AIAA Senior Member, millerd@mit.edu.

A. Motivation for Underactuated Tethered System

Accomplishing the goal of spiraling out and reaching some required level of UV plane coverage using the traditional thrusters leads to prohibitively high propellant usage. Beyond the fuel saving by employing tethered formation flight, this paper proposes a new actuation method, which further reduces the usage of propellant. In essence, we investigate the feasibility of controlling the array spin rate and relative attitude without thrusters. Such a tethered formation flight array without thrusters is characterized as an underactuated mechanical system. There are several advantages to the proposed underactuated control strategy. First, using reaction wheels instead of thrusters implies that power will be supplied via conversion of solar energy instead of carrying expensive propellant. We still envision using thrusters for out-of-plane motions,[4] but the life span of the mission would be greatly increased by using reaction wheels for controlling the array spin-rate. Second, the optics will not risk contamination by exhaust from the thrusters. The main application of tethered formation flight is stellar interferometry, and optics contamination should be avoided by all means.

B. Motivation for Decentralized Control and Estimation

Our decentralized control approach, first introduced in Ref. 5, is further generalized in this paper, in conjunction with nonlinear underactuated control. Our proposed method is unique in the sense that we use oscillation synchronization to simplify the coupled dynamics into the simplest form for which combined stability can be analyzed systematically (we refer the readers to Ref. 5 for further details). The importance of this approach lies with the fact that we can employ a fully decentralized control law (or estimation algorithm) from the reduced single-tether system to control a more complex multiple-spacecraft array, thereby reducing the complexity of both hardware and software (see Fig. 1). The decentralized controller will enable simple independent control of each satellite without the need for exchanging individual state information. This will significantly simplify both the control algorithm and hardware implementation as well as eliminating the possibility of performance degradation due to noisy and delayed communications.

C. Related Previous Work

We refer the readers to Ref. 4 and the references therein for prior work on tethered formation flight. It should be noted that previous work on tethered satellite formation flight is based upon the assumption that the tethered system is fully actuated whereas this article deals with underactuated tethered systems equipped with only reaction wheels. Control of underactuated mechanical systems is an active area of research.[1,3,13,14] In particular, Spong[17] developed the partial feedback linearization technique for the swing up maneuver of the acrobot. One drawback of the partial feedback linearization method is that it does not automatically guarantee stable zero dynamics after applying the change of control. Backstepping[8] is another alternative methodology to come up with an underactuated nonlinear controller. However, backstepping is applicable only to strict-feedback systems. A model reduction technique by transforming a class of underactuated systems to cascade normal forms is presented in Ref. 13. In addition, recent work examines the sliding-mode control,[23] intelligent control,[2] and hybrid switching control[25] for underactuated nonlinear systems. In the context of geometric control theory, two energy-based methods can be considered for underactuated nonlinear systems. First, an oscillatory control based on averaging[1,3] can be developed, which requires a high-frequency control input. The second geometric control approach is the method of controlled Lagrangians via the so-called matching process.[1] In essence, the control design involves shaping the system's total or kinetic energy with the additional parameters and the matching process. One drawback is that generic physical damping makes the control-modified energy rate indefinite, thus invalidating the nonlinear stability argument of the controlled Lagrangian method.[24] Since the SPHERES tethered formation flying experimental setup involves various forms of friction (see Ref. 4), the method of controlled Lagrangians is not pursued in this paper.

Control of underactuated spacecraft has also been a popular subject. Of particular interest is work by Tsiotras[19–21] showing that a nonsmooth time-invariant feedback control law can be used to rotate an axis-symmetric rigid spacecraft to the equilibrium using only two control torques.

Most aforementioned work is restricted to a single-body dynamics problem. In this paper, the decentralized control strategy from Ref. 5 is extended to the underactuated control of multi-vehicle tethered formation flying. To our knowledge, this work presents the first linear and nonlinear control results for underactuated tethered formation flight systems.

D. Organization

After reviewing some fundamental aspects of underactuated tethered systems in Section II, we first present gain-scheduled linear control in Section III. Then, we present nonlinear control laws based on feedback linearization via momentum decoupling (Section IV-A), and backstepping (Section IV-B). We show in Section IV-C that a fully decentralized control law designed from the underactuated single-tethered system can stabilize a multi-vehicle tethered array. Section VI discusses simulation results, where the nonlinear tracking control laws are compared with the linear control approach. In Section V, a new momentum dumping method that does not use torque-generating thrusters is presented. Experimental results using SPHERES nano-satellites are presented in Section VII.

II. Underactuated Tethered Formation Flight Spacecraft

We have proven in Ref. 5 that a fully decentralized control law designed from a single-tethered spacecraft can also stabilize arbitrarily large circular arrays of tethered spacecraft including a two-spacecraft configuration. Furthermore, due to the hierarchical combination, the dynamics of a three-inline configuration reduce to those of the single-tethered systems if the center spacecraft becomes exponentially stabilized by a simple independent control law (see Fig. 1). Consequently, we first focus on control of an underactuated single-tethered system (see Fig. 2(c)), and then discuss decentralization and decoupling in Section IV-C. To that end, we proceed to illustrate the dynamics and challenges of the underactuated single-tethered system.

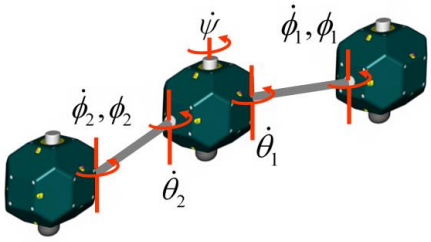

(a) Three inline configuration with a hierarchical combination

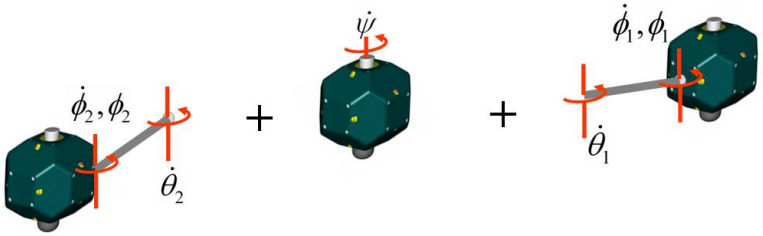

(b) Decoupled into two independent single-tethered systems and a center spacecraft

Figure 1. Three-spacecraft array decoupled into three sub-systems (see Ref. 5).

A. Fundamentals

Underactuated mechanical systems are characterized by fewer actuators than degrees of freedom (DOF) or configuration variables, and encountered in a wide range of applications such as walking robots,[18] aerospace vehicles,[6,13] and nonholonomic systems.[1] Popular two-DOF examples include the acrobot (Figure 2-(a)) and the pendubot (Figure 2-(b)), where the control input is available only to one joint variable. In contrast, the single-tethered system in Figure 2-(c) is underactuated via input coupling. This paper also serves the purpose of proposing the single-tethered system as another underactuated control benchmark problem. We also attempt to make a connection between the single-tethered system, which is a fundamental building block for constructing multi-spacecraft arrays, and a two-link planar robot, which has been a representative example in nonlinear control theory.

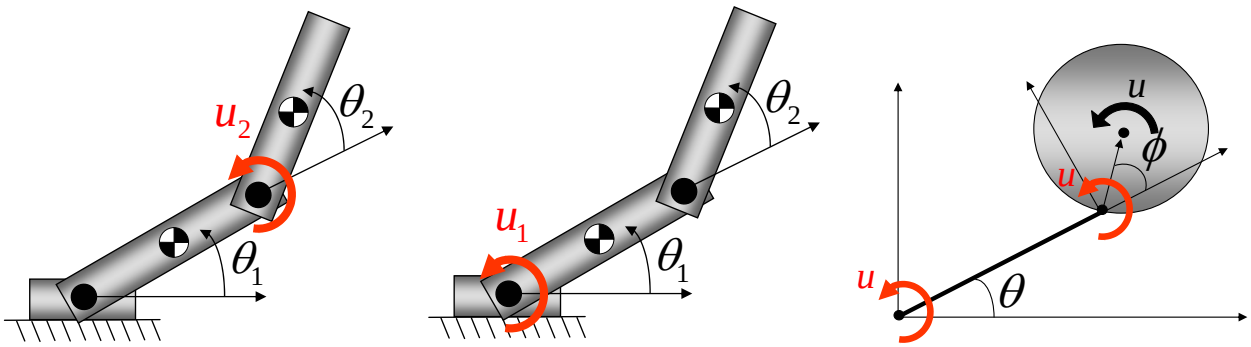

(a) Acrobot (b) Pendubot (c) Tethered-spacecraft without thrusters

Figure 2. Three representative cases of underactuated two-link mechanical systems.

The equations of motion for the singled-tethered system under the torque actuator only ($u \neq 0, F = 0$) becomes[4]

$$\mathbf{M_1}(\phi)\begin{pmatrix}\ddot{\theta}\\ \ddot{\phi}\end{pmatrix} + \mathbf{C_1}(\phi,\dot{\theta},\dot{\phi})\begin{pmatrix}\dot{\theta}\\ \dot{\phi}\end{pmatrix} = \begin{pmatrix}u\\ u\end{pmatrix} \tag{1}$$

where $\mathbf{M_1}(\phi) = \begin{bmatrix} m_{11}(\phi) & m_{12}(\phi) \\ m_{12}(\phi) & m_{22} \end{bmatrix} = \begin{bmatrix} I_r + m\ell^2 + 2mr\ell\cos\phi & I_r + mr\ell\cos\phi \\ I_r + mr\ell\cos\phi & I_r \end{bmatrix}$,

$\mathbf{C_1}(\phi,\dot{\theta},\dot{\phi}) = \begin{bmatrix} c_{11}(\phi,\dot{\phi}) & c_{12}(\phi,\dot{\theta},\dot{\phi}) \\ c_{21}(\phi,\dot{\theta}) & c_{22} \end{bmatrix} = \begin{bmatrix} -mr\ell\sin\phi\dot{\phi} & -mr\ell\sin\phi(\dot{\theta}+\dot{\phi}) \\ +mr\ell\sin\phi\dot{\theta} & 0 \end{bmatrix}$.

In the equations above, r, ℓ, and I_G denote the satellite's radius, tether length, and moment of inertia. I_r is the moment of inertia about the tether attachment point ($I_r = I_G + mr^2$). u denotes the torque exerted on the Center of Mass (CM) of the satellite, e.g. torque by a Reaction Wheel Assembly (RWA) or diagonal thruster firings.

Equation (1) clearly shows that the single input u enters both the configuration variables θ and ϕ, as opposed to the acrobot $\tau = \begin{pmatrix}0 & u\end{pmatrix}^T$ and the pendubot $\tau = \begin{pmatrix}u & 0\end{pmatrix}^T$. Even though all three cases in Figure 2 are derived from the two-link manipulator robot, there exists another fundamental difference. There is no gravity in the tethered system. In particular, underactuated mechanical systems such as the acrobot are in general not controllable in the absence of the gravity. However, the artificial gravity, induced by the centrifugal force of array rotation, plays a crucial role in making the tethered system controllable and stable.

B. Nonlinear Phase Portrait and Relative Equilibria

In this section, we investigate the qualitative pictures of the nonlinear trajectories of (1) by plotting a phase portrait. By looking at a phase portrait, stability and trajectory information from various initial conditions $(\phi(0), \dot{\phi}(0))$ is obtained.

We can multiply (1) by the inverse of the inertia matrix, $\mathbf{M}$ to get the equation of $\ddot{\phi}$. We assume that the system rotates at a constant angular velocity ($\dot{\theta} = \omega$). Then, the homogeneous equation of ϕ results in the following second-order differential equation:

$$\frac{d}{dt}\begin{pmatrix}\phi\\ \dot{\phi}\end{pmatrix} = \begin{pmatrix}\dot{\phi}\\ -\frac{r\sin\phi}{\ell(I_G+mr^2(\sin^2\phi))}\left[(I_r+mr\ell\cos\phi)(\dot{\theta}+\dot{\phi})^2 + mr\ell\dot{\theta}^2\cos\phi + m\ell^2\dot{\theta}^2\right]\end{pmatrix} \tag{2}$$

Figure 3-(a) shows a phase portrait of the nonlinear compound pendulum motion when the single tethered SPHERES revolves around the center of the inertial frame at a constant angular speed ($\dot{\theta} = \omega$). The following physical parameters are used: I_G=0.0213 kgm^2, m=4.5 kg, r=0.125 m , ω=0.3 rad/s, and ℓ=0.5 m. It correctly predicts a pendulum libration mode. When $\dot{\phi}$ is small enough, it oscillates in a closed circle or ellipse, which is a periodic orbit of the libration motion. However, a larger $\dot{\phi}$ leads to the ϕ rotation

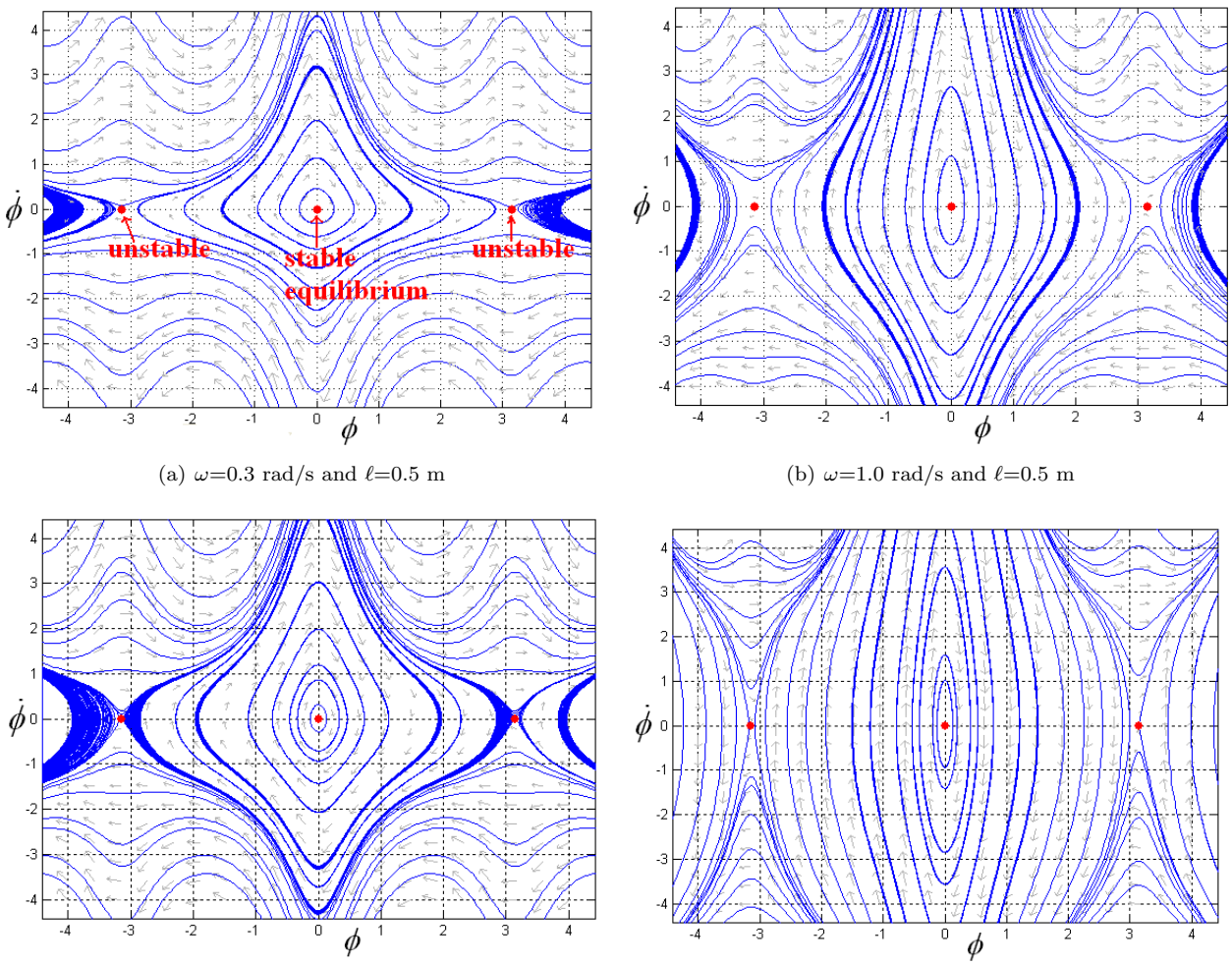

(a) ω=0.3 rad/s and ℓ=0.5 m

(b) ω=1.0 rad/s and ℓ=0.5 m

(c) ω=0.3 rad/s and ℓ=2.0 m

(d) ω=1.0 rad/s and ℓ=2.0 m

Figure 3. Phase portrait of (2). The dots indicate the relative equilibria

of spheres more than 180 degrees without being contained in a closed trajectory. In reality, it will hit the tether wire when ϕ crosses π rad. Since ω is positive (counterclockwise) rotation, the maximum value of $\dot{\phi}$ in a librational motion is greater when $\dot{\phi}$ has the same sign.

To investigate the effect of different tether lengths and angular rotational speeds, several phase plots are constructed. Figure 3-(b) shows a phase portrait with an increased angular velocity (ω=1.0 rad/s). We can see the region of a periodic orbit has been greatly expanded. A limit cycle becomes more towards the vertical $\dot{\phi}$ axis. A similar trend is observed when we increase the tether length ℓ, in Figures 3-(c) and (d).

There exist three equilibrium points in those phase portraits. Only $\phi = 0, \dot{\phi} = 0$ is a stable equilibrium. Along with the nominal array rotational rate, ω, the equilibria of (syseqn1) define the relative[3] equilibria of the spinning tethered array. Relative equilibria are commonly found in a spinning rigid body with symmetries. For the case of the three-dimensional free rigid body, the body is in relative equilibrium if and only if its angular velocity and angular momentum align, that is, if the body rotates about one of its principal axes.

C. Linearization and Pendulum Mode Frequency

We linearize (1) about the relative equilibrium point with $\dot{\theta} = \omega$, $\dot{\phi}$, and $\phi = 0$ where ω denotes a nominal angular rate. Each term can be linearized as the following: $mrl \sin\phi\dot{\theta}^2 \approx mrl\omega^2\phi, mrl \sin\phi\dot{\phi}^2 \approx$

$0, mrl\sin\phi\dot{\theta}\dot{\phi} \approx 0, \cos\phi \approx 1$. The linearized equation of the motion is presented:

$$\begin{bmatrix} I_G + m(r+\ell)^2 & I_G + mr(r+\ell) \\ I_G + mr(r+\ell) & I_G + mr^2 \end{bmatrix} \begin{pmatrix} \ddot{\theta} \\ \ddot{\phi} \end{pmatrix} + \begin{bmatrix} 0 & 0 \\ 0 & mr\ell\omega^2 \end{bmatrix} \begin{pmatrix} \theta \\ \phi \end{pmatrix} = \begin{bmatrix} r+\ell & 1 \\ r & 1 \end{bmatrix} \begin{pmatrix} F \\ u \end{pmatrix} \tag{3}$$

The nonzero rotational rate, $\dot{\theta}$, adds a potential term to the dynamics, even in the absence of gravity. This artificial potential energy induced by array rotation makes the system controllable and stable. This is especially true for large classes of underactuated systems (e.g. tethered systems with $F = 0$), which are neither controllable in the absence of potential energy nor fully feedback linearizable.[13]

A nice property about this linearized equation (3) is that we can decouple the equation of ϕ from that of θ. The first equation is merely the dynamics of a rigid body mode of θ. The frequency of the pendular libration mode is computed as

$$\omega_\phi = \sqrt{\frac{r(I_G + m(r+\ell)^2)}{\ell I_G}}\omega = \sqrt{\frac{r(I_r + m\ell(2r+\ell))}{\ell I_G}}\omega \quad [\text{rad/s}] \tag{4}$$

The faster the array spins, the higher the pendulum mode becomes. The tether length ℓ also increases the pendulum mode frequency past the global minimum. The actual raw gyro data from a single tethered SPHERES exhibits the high frequency oscillation (the compound pendulum mode, $\dot{\phi}$) and the DC component (the rigid body mode of the rotational rate, $\dot{\theta}$). The frequency obtained by (4) correctly predicted the actual oscillation frequency obtained from the gyro measurement (see Ref. 4).

D. Controllability Test

The linearized system of a single-tethered spacecraft, rotating at a constant $\dot{\theta} = \omega$, is derived from (3) as the following.

$$\frac{d}{dt}\begin{pmatrix} \theta \\ \phi \\ \dot{\theta} \\ \dot{\phi} \end{pmatrix} = \begin{bmatrix} 0 & 0 & 1 & 0 \\ 0 & 0 & 0 & 1 \\ 0 & \frac{r\omega^2\left(I_G + mr(r+\ell)\right)}{\ell I_G} & 0 & 0 \\ 0 & -\frac{r\omega^2\left(I_G + m(r+\ell)^2\right)}{\ell I_G} & 0 & 0 \end{bmatrix} \begin{pmatrix} \theta \\ \phi \\ \dot{\theta} \\ \dot{\phi} \end{pmatrix} + \begin{bmatrix} 0 \\ 0 \\ -\frac{r}{I_G\ell} \\ \frac{r+\ell}{I_G\ell} \end{bmatrix} u \tag{5}$$

where the first matrix of the righthand side is the 4×4 system matrix A and the second is the 4×2 input matrix B. Note that θ is easily eliminated by removing the first column and the first of row of A matrix, thereby reducing the dimension to three.

We can check if all the states (θ,ϕ,$\dot{\theta}$,$\dot{\phi}$) are controllable only by the torque generating actuator u (e.g. RWA). The controllability matrix using the second column of B matrix in (5), $\mathcal{C} = \begin{bmatrix} B_2 & AB_2 & A^2B_2 & A^3B_2 \end{bmatrix}$ becomes:

$$\mathcal{C} = \begin{bmatrix} 0 & -\frac{r}{I_G\ell} & 0 & \frac{r(r+\ell)\omega^2\left(I_G + mr(r+\ell)\right)}{\ell^2 {I_G}^2} \\ 0 & \frac{r+\ell}{I_G\ell} & 0 & -\frac{r(r+\ell)\omega^2\left(I_G + m(r+\ell)^2\right)}{l^2 {I_G}^2} \\ -\frac{r}{I_G\ell} & 0 & \frac{r(r+\ell)\omega^2\left(I_G + mr(r+\ell)\right)}{\ell^2 {I_G}^2} & 0 \\ \frac{r+l}{I_G\ell} & 0 & -\frac{r(r+\ell)\omega^2\left(I_G + m(r+\ell)^2\right)}{\ell^2 {I_G}^2} & 0 \end{bmatrix} \tag{6}$$

This is a full rank ($n = 4$) matrix for any nonzero ω and tether length, ℓ. Since its linear approximation is controllable, under some mild smoothness assumptions, the nonlinear system can be driven from any point in a closed connect region U to any point in U. Its implication to the future tethered systems is significant: the tethered satellite systems are able to spin up and re-size the array without the use of propellant consumable when operating around the relative equilibrium of a nominal array angular rate, $\dot{\theta} = \omega$. The underactuated controllers, introduced in this article takes advantage of this observation. It should be noted that the controllability matrix $\mathcal{C}$ tends to a singular matrix as the tether length ℓ tends to infinity. For example, Figure 4 shows that the condition number of the controllability matrix using the physical parameters of the SPHERES testbed (see VII). This result implies that the underactuated system using only torque input goes less controllable as the tether length increases.

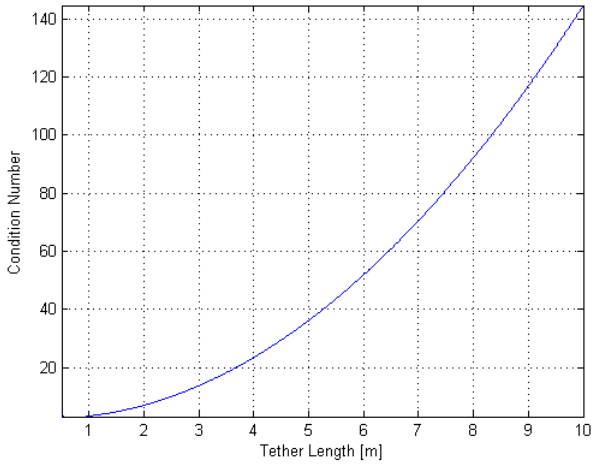

Figure 4. Condition number of the controllability matrix for the tethered SPHERES

E. Challenges of Nonlinear Underactuated Systems

As mentioned earlier, an underactuated mechanical system is not, in general, exactly input-state feedback linearizable. Its lack of feedback linearizability, along with its complex nonholonomic behavior, characterizes the difficult nonlinear control problem. It has been shown in Ref. 12 that the acrobot is not feedback linearizable with static state feedback and nonlinear coordinate transformation. In this section, we derive a similar result for the single tethered system given in Eq. (1) and Fig. 2(c).

Consider a nonlinear system, affine in the control input u, with $\mathbf{f}(\mathbf{x})$ and $\mathbf{g}(\mathbf{x})$ being smooth vector fields,

$$\dot{\mathbf{x}} = \mathbf{f}(\mathbf{x}) + \mathbf{g}(\mathbf{x})u \tag{7}$$

The system is input-state linearizable[16] in an open set U such that a nonlinear feedback control law $u = \alpha(\mathbf{x})v + \beta(\mathbf{x})$ and a diffeomorphism $\mathbf{z} = \phi(\mathbf{x})$, transform Eq. (7) to the resultant linear dynamics

$$\dot{\mathbf{z}} = \mathbf{A}\mathbf{z} + \mathbf{b}v \tag{8}$$

if and only if (1) dim span$\{g, ad_f g, \cdots, ad_f^{n-1} g\}(\mathbf{x}) = n$, $\forall \mathbf{x} \in U$ in $\mathbb{R}^n$– i.e., the vector fields are linearly independent. and (2) span$\{g, ad_f g, \cdots, ad_f^{n-2} g\}$ is an involutive distribution on U. Note that $ad_f^i g$ is the iterated Lie bracket $[f, \cdots, [f, g] \cdots]$.

We can easily write the dynamics of the single-tethered system in the first-order form, shown in Eq. (7), by multiplying Eq. (1) with the inverse of the inertia matrix, $\mathbf{M_1}(\phi)$. The underactuated tethered system in Eq. (1) satisfies the first condition, which corresponds to a controllability test. This result agrees with the linear controllability analysis about the relative equilibria, as discussed in Section D. The more subtle second condition, derived by Frobenius' theorem, warrants further discussion. To meet the involutivity condition, the following vector fields

$$[g, ad_f g] \quad [g, ad_f^2 g] \quad [ad_f g, ad_f^2 g] \tag{9}$$

must lie in the distribution $\Delta = \text{span}\{g, ad_f g, ad_f^2 g\}$. It is verified in Ref. 4 via Mathematica that the matrix constructed by one of the above vector fields and Δ has full rank of four. This in turn implies that they do not lie in the distribution Δ (all vectors are independent). As a result, similar to the acrobot, the underactuated single-tethered system fails the involutivity test, and hence is not input-state feedback linearizable.

Nevertheless, there might exist an output function to render input-output feedback linearizability. Finding such an output function is not trivial, and additional work is required to ensure that the associated zero dynamics are stable. This is one of the reasons that designing an efficient control law of a large class of underactuated systems is generally an open problem. In Section IV-A, we introduce a nonlinear diffeomorphism that permits model reduction and simple feedback linearization about the transformed state vector, inspired by the following normal forms.[13]

F. Normal Forms for Underactuated Systems

Olfati-Saber[13] developed cascade normal forms for underactuated mechanical systems, based upon the mechanical symmetry. Normal forms can be further classified into triangular normal forms and nontriangular forms. Both strict-feedback and strict-feedforward systems are called "triangular" by analogy with linear systems. In particular, a strict-feedback system permits a systematic nonlinear control design called backstepping.

Let us consider the dynamics similar to the acrobot such that the input is applied only to the shape variable q_2:

$$\begin{aligned} m_{11}(q_2)\ddot{q}_1 + m_{12}(q_2)\ddot{q}_2 + h_1(q_1, q_2, \dot{q}_1, \dot{q}_2) &= 0 \\ m_{21}(q_2)\ddot{q}_1 + m_{22}(q_2)\ddot{q}_2 + h_2(q_1, q_2, \dot{q}_1, \dot{q}_2) &= \tau \end{aligned} \tag{10}$$

where the dynamics are kinetic symmetric with respect to q_2 such that $m_{ij}(\mathbf{q}) = m_{ij}(q_2)$.
Similar to the partial linearization, there exists an invertible change of control input $\tau = \alpha(\mathbf{q})u + \beta(\mathbf{q}, \dot{\mathbf{q}})$, which transforms the dynamics into

$$\begin{aligned} \dot{q}_1 &= p_1 \\ \dot{p}_1 &= -m_{11}^{-1}(q_2)h_1(q_1, q_2, p_1, p_2) - m_{11}^{-1}(q_2)m_{12}(q_2)u \\ \dot{q}_2 &= p_2 \\ \dot{p}_2 &= u \end{aligned} \tag{11}$$

Since the linearization was performed on the actuated variable q_2, such a change of control is called collocated partial feedback linearization. Ref. 13 introduces a diffeomorphism transforming the above equation into a strict-feedback form:

$$\begin{aligned} \dot{z}_1 &= m_{11}^{-1}(\xi_1)z_2 \\ \dot{z}_2 &= g(z_1, \xi_1) \\ \dot{\xi}_1 &= \xi_2 \\ \dot{\xi}_2 &= u \end{aligned} \tag{12}$$

where $g(\cdot, \cdot)$ is the gravity term. Unfortunately, the single-tethered system shown in Fig. 2(c) does not permit the same strict-feedback form due to its input coupling and the lack of such a gravity function. Nevertheless, in Section IV-A, we show that the same transformation yields a useful coordinate transformation permitting feedback linearization and backstepping control design for the reduced variables z_1 and z_2.

We can also show that the pendubot in Fig. 2(b) can be transformed into a cascade nonlinear system in nontriangular quadratic normal form by a similar transformation. Stabilization of a nontriangular form, addressed in Ref. 13, is in general much more difficult than that of a triangular form. For example, backstepping or forwarding[13] is not applicable. Even though the single-tethered dynamics in Fig. 2 can be transformed into a non-triangular form, such a method is not pursued in this paper due to the challenge associated with a nontriangular form. Instead, we apply feedback linearization and backstepping to the reduced system by using a transformation similar to Eq. (12).

III. Gain-Scheduled LQR Approach

Even though we embraced this linear control technique in the actual implementation in Section VII, for simplicity, we emphasize that the linearization-based control would only provide a local stability result, as opposed to global convergence of the nonlinear control strategies introduced in the subsequent sections. Again, the controllability analysis in Section II-D states that the spinning underactuated tethered system is fully controllable around the relative equilibrium manifold ($\dot{\theta} = \omega$, $\phi = 0$, and $\dot{\phi} = 0$). This indicates that the configuration variable ϕ is not subject to a large angle rotation as seen in a swing-up maneuver of the acrbot, but rather has to be stabilized at the equilibrium $\phi = 0, \dot{\phi} = 0$ at all times. Thanks to this requirement, we can expect that the linear LQR control can perform reasonably well around the equilibrium point.

Recalling that the linearized equations in Eq. (5) are fully controllable using only the torque input u, we can construct a linear feedback control law $u = K(\phi, \dot{\theta}, \dot{\phi})$, based upon the following linearized equations of motion:

$$\frac{d}{dt}\begin{pmatrix}\phi\\ \dot{\theta}\\ \dot{\phi}\end{pmatrix} = \begin{bmatrix} 0 & 0 & 1\\ \frac{r\omega^2\left(I_r+mr\ell\right)}{\ell I_G} & 0 & 0\\ -\frac{r\omega^2\left(I_r+m\ell(2r+\ell)\right)}{\ell I_G} & 0 & 0\end{bmatrix}\begin{pmatrix}\phi\\ \dot{\theta}\\ \dot{\phi}\end{pmatrix} + \begin{pmatrix}0\\ -\frac{r}{I_G\ell}\\ \frac{r+\ell}{I_G\ell}\end{pmatrix} u \tag{13}$$

where we intentionally left out the state θ since it is merely a rigid body rotation mode.
We assume that all the states $(\phi, \dot{\theta}, \dot{\phi})$ are available by the estimator described in Ref. 4. Then, we can design a Linear Quadratic Regulator (LQR) controller, which specifically addresses the issue of achieving a balance between good system response and minimizing the control effort required. The LQR control also possesses very good stability margins.

Since the A matrix in Eq. (13) is a function of $\dot{\theta}$ and the tether length ℓ, the optimal LQR gains are computed for a range of angular rates and tether lengths. A continuous function is then fit to these discrete gains. Then, the gain-scheduled LQR gain is a continuous function of $\dot{\theta}$ and tether length ℓ as depicted in Fig. 5:

$$u = -K_1(\dot{\theta}, \ell)\phi - K_2(\dot{\theta} - \dot{\theta}_d) - K_3(\dot{\theta}, \ell)\dot{\phi} \tag{14}$$

where K_2 turns out to be independent of $\dot{\theta}$ and ℓ.

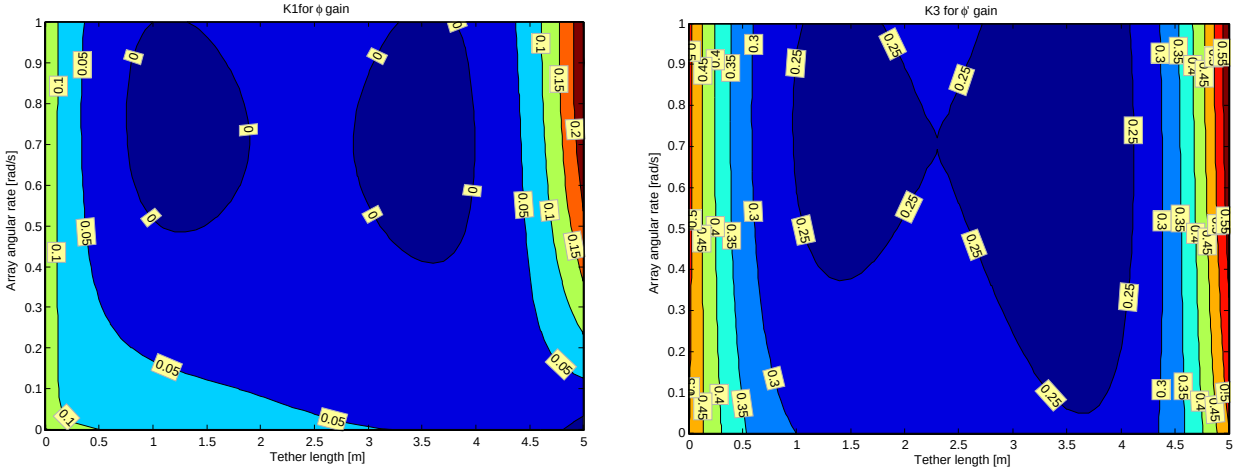

(a) K1 for ϕ

(b) K3 for $\dot{\phi}$

Figure 5. LQR gains scheduled for a range of $\dot{\theta}$ and ℓ

Such a gain-scheduled LQR controller has been successfully implemented in the SPHERES testbed, as shall be seen in Section VII. This gain-scheduling approach has been a popular subject of research as alternative form of nonlinear control, as indicated in a recent survey paper.[15] One merit of the linearization is that it permits the use of mature and well-established linear control techniques to address nonlinear problems. However, stability can be assured only locally and in a "slow-variation" setting.[15] In Section IV, we present several nonlinear control techniques, yielding global stability results.

A. Stability of Decentralized Linear Control

It is shown in Ref. 5 that a linear decentralized control in Eq. (14)

$$\begin{aligned} u_1 &= -K_1\phi_1 - K_2(\dot{\theta} - \dot{\theta}_d) - K_3\dot{\phi}_1\\ u_2 &= -K_1\phi_2 - K_2(\dot{\theta} - \dot{\theta}_d) - K_3\dot{\phi}_2 \end{aligned} \tag{15}$$

stabilizes the linearized tethered two-spacecraft dynamics in Eq. (13) if $rK_2 < (r+\ell)K_3,\ K_1 > 0,\ K_2 > 0$. Furthermore, it is proven that such a decentralized control synchronizes the compound pendulum oscillation, ϕ_1 and ϕ_2. Consequently, we can stabilize a coupled tethered array without the need for any inter-satellite

communication, thereby reducing the complexity in both the hardware and software. We can also expect that the decentralized control techniques introduced in this section possess the same stability property for a multi-vehicle underactuated system if the behavior of the closed-loop systems is sufficiently close to the linearized dynamics. In the case of spinning tethered arrays, this is particularly true for a regulatory control in which a desired trajectory is time-invariant. Note that the stability proof of decentralized nonlinear control for underactuated tethered spacecraft is more involved and presented in Section IV-C.

IV. Nonlinear Underatuated Control

We introduce two nonlinear control methods, based on the momentum decoupling.

A. Momentum Decoupling and Feedback Linearization of Reduced Models

Even though exact feedback linearization is not possible for an underactuated tethered system, as discussed in Section E, we show herein that there exists a diffeomorphism such that feedback linearization is made possible with respect to the relative equilibria of a spinning tethered system.

We recall the dynamics of the underactuated single-tethered system with the fixed tether length from (1):

$$\begin{aligned}\frac{d}{dt}\frac{\partial L}{\partial \dot{\theta}} - \frac{\partial L}{\partial \theta} &= m_{11}\ddot{\theta} + m_{12}\ddot{\phi} + c_{11}\dot{\theta} + c_{12}\dot{\phi} = u \\ \frac{d}{dt}\frac{\partial L}{\partial \dot{\phi}} - \frac{\partial L}{\partial \phi} &= m_{21}\ddot{\theta} + m_{22}\ddot{\phi} + c_{21}\dot{\theta} + c_{22}\dot{\phi} = u\end{aligned} \tag{16}$$

Following Ref. 13, consider the nonlinear diffeomorphism applying the change of coordinates such that

$$\begin{aligned}z_1 &= \theta + \gamma(\phi) \\ z_2 &= m_{11}(\phi)\dot{\theta} + m_{12}(\phi)\dot{\phi}\end{aligned} \tag{17}$$

where

$$\gamma = \int_0^{\phi} \frac{m_{12}(s)}{m_{11}(s)} ds = \int_0^{\phi} \frac{I_r + mr\ell\cos(s)}{I_r + m\ell^2 + 2mr\ell\cos(s)} ds. \tag{18}$$

The kinetic symmetry with respect to θ in the absence of a gravitational effect leads to symmetry in mechanics such that

$$\frac{\partial K}{\partial \theta} = \frac{\partial L}{\partial \theta} = 0 \tag{19}$$

since the corresponding Lagrangian, L is independent of θ.

z_2 is essentially the first generalized angular momentum such that

$$z_2 = \frac{\partial L}{\partial \dot{\theta}}, \qquad \dot{z}_2 = \frac{d}{dt}\frac{\partial L}{\partial \dot{\theta}} = \frac{\partial L}{\partial \theta} + u = u \tag{20}$$

In addition,

$$\dot{z}_1 = \dot{\theta} + \frac{m_{12}(\phi)}{m_{11}(\phi)}\dot{\phi} = \frac{m_{11}(\phi)\dot{\theta} + m_{12}(\phi)\dot{\phi}}{m_{11}(\phi)} = \frac{z_2}{m_{11}(\phi)} \tag{21}$$

Incorporating Equations (21) and (20), we obtain the following equations of z_1 and z_2:

$$\begin{aligned}\dot{z}_1 &= m_{11}^{-1}(\phi) z_2 \\ \dot{z}_2 &= u\end{aligned} \tag{22}$$

where $m_{11}(\phi) = I_r + m\ell^2 + 2mr\ell\cos\phi$. Note that $m_{11}(\phi) > 0,\ \forall\phi$ since $I_r = I_G + mr^2$.

A closer examination of the definition of z_1 and z_2 given in (17) reveals that z_1 corresponds to a superposition of two angular variables, θ and ϕ, whereas z_2 is the generalized momentum conjugate to θ.

By differentiating $\dot{z}_1$,

$$\begin{aligned}\ddot{z}_1 &= \left[\frac{\partial m_{11}^{-1}(\phi)}{\partial \phi}\dot{\phi} z_2\right] + m_{11}^{-1}(\phi)\dot{z}_2 \\ &= \frac{2mr\ell \sin\phi}{(I_r + m\ell^2 + 2mr\ell\cos\phi)^2}\dot{\phi} z_2 + m_{11}^{-1}(\phi)u \\ &= v\end{aligned} \tag{23}$$

The following definition of the new control input v guarantees exponential convergence of z_1 to z_{1d}:

$$v = \ddot{z}_{1d} - D(\dot{z}_1 - \dot{z}_{1d}) - K(z_1 - z_{1d}) \tag{24}$$

where K and D are positive constants.

For $\phi_d = 0$ and $\dot{\phi}_d = 0$, the reference $\dot{z}_{1d}$ and $\ddot{z}_{1d}$ can be defined as

$$\dot{z}_{1d} = m_{11}^{-1}(\phi) z_{2d} = m_{11}^{-1}(\phi)\left(m_{11}(\phi)\dot{\theta}_d + m_{12}(\phi)\dot{\phi}_d\right) = \dot{\theta}_d, \quad \ddot{z}_{1d} = \ddot{\theta}_d \tag{25}$$

For the error $(z_1 - z_{1d})$, we are mainly concerned with the array angular rate $\dot{\theta}$ of the spinning tethered array, so we consider only the $\gamma(\phi)$ term in z_1 such that

$$z_1 - z_{1d} \approx \gamma(\phi) - \gamma(\phi_d) = \gamma(\phi) \tag{26}$$

where $\gamma(\phi)$ is analytically obtained from the integral in (17) using Mathematica:

$$\begin{aligned}\gamma(\phi) &= \int_0^\phi \frac{m_{12}(s)}{m_{11}(s)} ds = \int_0^\phi \frac{I_r + mr\ell\cos(s)}{I_r + m\ell^2 + 2mr\ell\cos(s)} ds \\ &= \frac{\phi}{2} + \frac{m\ell^2 - I_r}{\sqrt{-(m\ell^2 + I_r)^2 + 4m^2r^2\ell^2}} \tanh^{-1}\left(\frac{I_r + m\ell(\ell - 2r)}{\sqrt{-(m\ell^2 + I_r)^2 + 4m^2r^2\ell^2}} \tan\frac{\phi}{2}\right)\end{aligned} \tag{27}$$

Figure 6 plots the function $\gamma(\phi)$ in Eq. (27), which is a monotonic function of ϕ within a small range of the compound pendulum mode angle ϕ.

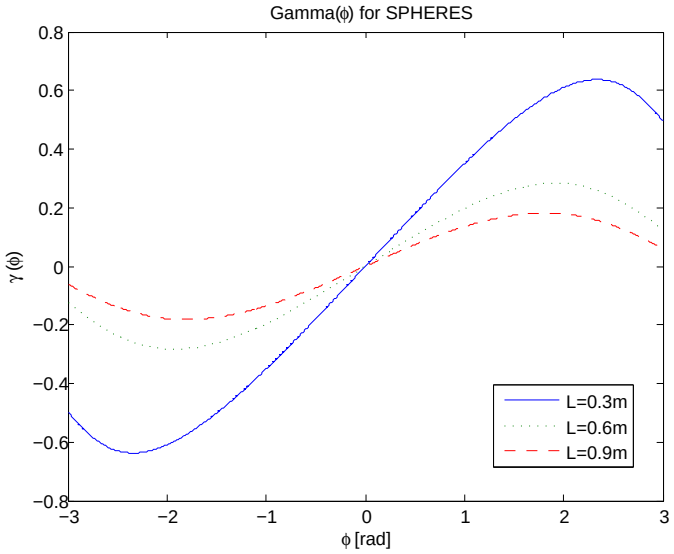

Figure 6. Plot of $\gamma(\phi)$ using ℓ=(0.3m, 0.6m, 0.9m) and the SPHERES physical parameters.

From (23), the original torque input u can be computed:

$$u = m_{11}(\phi)v - \frac{2mr\ell\sin\phi}{m_{11}(\phi)}\dot{\phi} z_2 \tag{28}$$

where the new control input v is defined in (24).

As discussed in Section E, the original nonlinear system in (1) is not fully feedback linearizable with respect to its states, $\theta, \dot{\theta}, \phi, \dot{\phi}$. Nonetheless, the nonlinear control law in (28) using feedback linearization is made possible with respect to the reduced variables, z_1 and z_2. The simulation results in Section VI shows that (28) is particularly efficient for tracking the desired trajectory of $\dot{\theta}_d$ while the desired ϕ_d and $\dot{\phi}_d$ are set to zero.

B. Tracking Control by Backstepping and Contraction Analysis

Feedback linearization often results in cancellations of useful nonlinearities. To the contrary, backstepping design is more flexible and does not force the designed system to appear linear. This implies that backstepping can avoid cancellations of useful nonlinearities and often introduce additional nonlinear terms to improve transient performance.[8] We present a backstepping nonlinear control design of the single tethered system, based upon the strict-feedback cascade normal form introduced n the previous section.

Recalling the reduced dynamics of z_1 and z_2 from (22),

$$\begin{aligned} \dot{z}_1 &= m_{11}^{-1}(\phi) z_2 \\ \dot{z}_2 &= u \end{aligned} \tag{29}$$

This is in strict-feedback form regarding (ϕ) as an exogenous variable, hence allows for backstepping.

Let us define the stabilizing function $\alpha(z_1) = -c_1 z_1$, $c_1 > 0$ such that the dynamics

$$\dot{z}_1 = m_{11}^{-1}(\phi)\alpha \tag{30}$$

is asymptotically stable with $V = \frac{1}{2}{z_1}^2$. Let us define the error function e such that

$$e = z_2 - \alpha(z_1) = z_2 + c_1 z_1 \tag{31}$$

and its time derivative is

$$\dot{e} = \dot{z}_2 + c_1 \dot{z}_1 = u + c_1 m_{11}^{-1}(\phi)(e - c_1 z_1). \tag{32}$$

Supposed that a CLF, V_a of the z_1 and z_2 dynamics is $V_a = \frac{1}{2}{z_1}^2 + \frac{1}{2}e^2$. Its time derivative should be bounded by the positive definite function $W(\mathbf{x})$ for asymptotic stability.

$$\begin{aligned} \dot{V}_a = z_1 \dot{z}_1 + e\dot{e} &= z_1 m_{11}^{-1}(\phi)(e - c_1 z_1) + e[u + c_1 m_{11}^{-1}(\phi)(e - c_1 z_1)] \\ &= -c_1 m_{11}^{-1}(\phi){z_1}^2 + e[u + c_1 m_{11}^{-1}(\phi)e + (1 - {c_1}^2)m_{11}^{-1}(\phi)z_1] \end{aligned} \tag{33}$$

The following u renders $\dot{V}_a = -c_1 m_{11}^{-1}(\phi){z_1}^2 - c_2 e^2 < 0$ with $c_2 > 0$:

$$\begin{aligned} u &= -c_2 e - c_1 m_{11}^{-1}(\phi)e + ({c_1}^2 - 1)m_{11}^{-1}(\phi)z_1 \\ &= -[c_2 c_1 + m_{11}^{-1}(\phi)]z_1 - [c_2 + m_{11}^{-1}(\phi)c_1]z_2 \end{aligned} \tag{34}$$

The closed-loop system in the (z_1, e) coordinates results in

$$\begin{pmatrix} \dot{z}_1 \\ \dot{e} \end{pmatrix} = \begin{bmatrix} -c_1 m_{11}^{-1}(\phi) & m_{11}^{-1}(\phi) \\ -m_{11}^{-1}(\phi) & -c_2 \end{bmatrix} \begin{pmatrix} z_1 \\ e \end{pmatrix} \tag{35}$$

where c_1 and c_2 are positive constants.

The above equation shows an interesting property. The system matrix is uniformly (independent of time) negative definite due to the skew-symmetric off-diagonal terms and the positive $m_{11}(\phi)$ term. Possessing such a negative-definite system matrix is an important characteristic of backstepping design (see[8]). It is emphasized that a similar discussion automatically leads to contraction analysis.[10] The resulting equation of (z_1, e) in (35) is contracting due to its uniformly negative definite Jacobian, hence $(0, 0)$ is an exponentially stable equilibrium of (z_1, e). Since we are more interested in tracking control of the underactuated system, the following tracking control law is suggested based upon (35):

$$u = -[c_2 c_1 + m_{11}^{-1}(\phi)]z_1 - [c_2 + m_{11}^{-1}(\phi)c_1](z_2 - z_{2d}) + \dot{z}_{2d} \tag{36}$$

where $z_{2d} = m_{11}(\phi)\dot{\theta}_d$ and $\dot{z}_{2d} = m_{11}(\phi)\ddot{\theta}_d$ due to $\phi_d = 0, \dot{\phi}_d = 0$. Since we focus on the angular rate $\dot{\theta}$, z_{1d} is defined such that $z_1 - z_{1d} = z_1$ and $\dot{z}_{1d} = m_{11}^{-1}(\phi)z_{2d}$. Additionally, we set $e_d = z_{2d} + c_1 z_{1d}$ and $\dot{e}_d = \dot{z}_{2d} + c_1 \dot{z}_{1d}$. Then, the control law in Eq. (36) leads to the closed-loop system of the virtual variables y_1 and y_2, which has $\begin{pmatrix} y_1 & y_2 \end{pmatrix}^T = \begin{pmatrix} z_1 - z_{1d} & e - e_d \end{pmatrix}^T$ and $\begin{pmatrix} y_1 & y_2 \end{pmatrix}^T = \begin{pmatrix} 0 & 0 \end{pmatrix}^T$ as particular solutions. Its virtual displacement equation results in

$$\begin{pmatrix} \delta\dot{y}_1 \\ \delta\dot{y}_2 \end{pmatrix} = \begin{bmatrix} -c_1 m_{11}^{-1}(\phi) & m_{11}^{-1}(\phi) \\ -m_{11}^{-1}(\phi) & -c_2 \end{bmatrix} \begin{pmatrix} \delta y_1 \\ \delta y_2 \end{pmatrix}. \tag{37}$$

This is contracting, hence all solutions of y_1 and y_2 tend to each other, resulting in $\dot{\theta} \to \dot{\theta}_d$ and $\phi, \dot{\phi} \to 0$ from the definition of z_1, z_2 and e. Furthermore, the contraction rate of z_1 is proportional to c_1 whereas c_2 independently determines contraction rate of e. This indicates that we can properly tune the gains c_1 and c_2 for a desired performance of z_1 and z_2.

C. Decentralized Nonlinear Control For Multi-Vehicle Systems

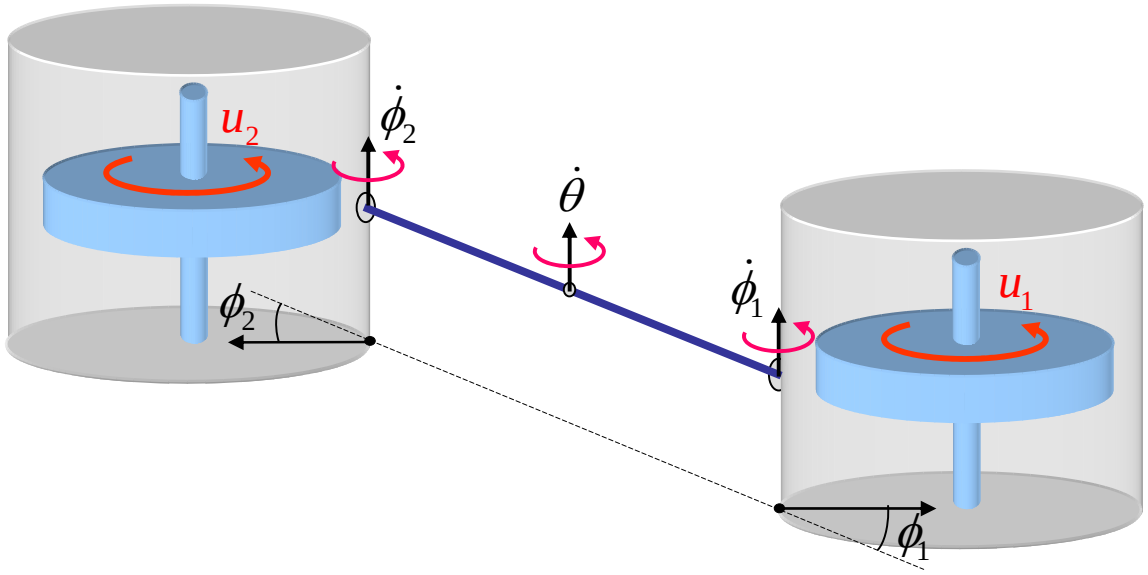

Figure 7. Two-spacecraft tethered system with a reaction wheel, depicted on the rotation plane. The ϕ_1 and ϕ_2 angles indicate the compound pendulum modes.

Following the model reduction technique introduced in Ref. 5, we show herein that a fully decentralized control law designed from the underactuated single-tethered system can stabilize a multi-vehicle tethered array. The decentralized controller will enable simple independent control of each satellite by eliminating the need for exchanging individual state information. This will significantly simplify both the control algorithm and hardware implementation, as well as eliminate any possibility of performance degradation due to noisy and delayed communications.

Consider a two-spacecraft array with only torque input (u_1, u_2), as illustrated in Fig. 7:

$$\mathbf{M_2}(\phi_1, \phi_2) \begin{pmatrix} \ddot{\theta} \\ \ddot{\phi}_1 \\ \ddot{\phi}_2 \end{pmatrix} + \mathbf{C_2}(\phi_1, \phi_2, \dot{\theta}, \dot{\phi}_1, \dot{\phi}_2) \begin{pmatrix} \dot{\theta} \\ \dot{\phi}_1 \\ \dot{\phi}_2 \end{pmatrix} = \begin{pmatrix} u_1 + u_2 \\ u_1 \\ u_2 \end{pmatrix} \tag{38}$$

where

$$\mathbf{M_2}(\phi_1,\phi_2) = \begin{bmatrix} m_{11}(\phi_1)+m_{11}(\phi_2) & m_{12}(\phi_1) & m_{12}(\phi_2) \\ m_{12}(\phi_1) & m_{22} & 0 \\ m_{12}(\phi_2) & 0 & m_{22} \end{bmatrix},$$
$$\mathbf{C_2}(\phi_1,\phi_2,\dot\theta,\dot\phi_1,\dot\phi_2) = \begin{bmatrix} c_{11}(\phi_1,\dot\phi_1)+c_{11}(\phi_2,\dot\phi_2) & c_{12}(\phi_1,\dot\theta,\dot\phi_1) & c_{12}(\phi_2,\dot\theta,\dot\phi_2) \\ c_{21}(\phi_1,\dot\theta) & c_{22} & 0 \\ c_{21}(\phi_2,\dot\theta) & 0 & c_{22} \end{bmatrix} \tag{39}$$

and m_{ij} and c_{ij} are defined in the single-tethered dynamics in Eq. (1).

We can proceed to prove the stability of the nonlinear decentralized control law introduced in Section IV-A. The proof entails showing that such a decentralized control law can de facto synchronize the two compound pendulum mode angles– ϕ_1 and ϕ_2 for the two-spacecraft system. Recall that the second and third rows of Eq. (38) are the independent dynamics for ϕ_1 and ϕ_2, respectively:

$$\begin{aligned} (I_r + mr\ell\cos\phi_1)\ddot\theta + I_r\ddot\phi_1 + mr\ell\dot\theta^2\sin\phi_1 = u_1 \\ (I_r + mr\ell\cos\phi_2)\ddot\theta + I_r\ddot\phi_2 + mr\ell\dot\theta^2\sin\phi_2 = u_2 \end{aligned} \tag{40}$$

where the decentralized control law u_i, $i = 1, 2$ from Eq. (28) can be written as

$$u_i = m_{11}(\phi_i)[\ddot\theta_d - D(\dot\theta - \dot\theta_d)] - Dm_{12}(\phi_i)\dot\phi_i - Km_{11}(\phi_i)\gamma(\phi_i) - \frac{2mr\ell\sin\phi_i}{m_{11}(\phi_i)}\dot\phi_i z_2(\phi_i) \tag{41}$$

Since the ϕ angle is stabilized ($\phi \to 0$), assume that ϕ and $\dot\phi$ are sufficiently small such that $m_{11}(\phi) \approx m_{11}(0)$, $\cos\phi \approx 1$, and $\sin\phi\dot\phi \approx 0$. Then, the closed-loop dynamics in Eq. (40) can be simplified as

$$\begin{aligned} I_r\ddot\phi_1 + Dm_{12}(\phi_1)\dot\phi_1 + Km_{11}(\phi_1)\gamma(\phi_1) + mr\ell\dot\theta^2\sin\phi_1 = g(t) \\ I_r\ddot\phi_2 + Dm_{12}(\phi_2)\dot\phi_2 + Km_{11}(\phi_2)\gamma(\phi_2) + mr\ell\dot\theta^2\sin\phi_2 = g(t) \end{aligned} \tag{42}$$

where the common excitation input is defined as

$$g(t) = -(I_r + mr\ell)\ddot\theta + m_{11}(0)[\ddot\theta_d - D(\dot\theta - \dot\theta_d)] \tag{43}$$

Also, note that $m_{11}(\phi) > 0\ \forall\phi$ and $m_{12}(\phi) > 0$ for $|\phi| < \frac{\pi}{2}$.

Consider the virtual dynamics of y that has ϕ_1 and ϕ_2 as its particular solutions:

$$I_r\ddot y + Dm_{12}(y)\dot y + Km_{11}(y)\gamma(y) + mr\ell\dot\theta^2\sin y = g(t) \tag{44}$$

The above dynamics is contracting ($\delta y \to 0$) with $D > 0$ and $K > 0$ in the region $|\phi| < \frac{\pi}{2}$, indicating that any solutions of y converge to each other. This in turn implies that ϕ_1 tends to ϕ_2 exponentially fast. Once $\phi_1 \to \phi_2$, it is straightforward to show that the equation of motion for two-spacecraft in Eq. (38) reduces to the superposition of the reduced variables z_1 and z_2 for each spacecraft. As a result, a decentralized control law designed form the single-tethered dynamics not only stabilizes the coupled two-spacecraft dynamics, but also synchronizes the compound pendulum mode angles ϕ_1 and ϕ_2. Following the discussion in Ref. 5, the above result can be extended to a triangular configuration and a three-inline configuration. In particular, due to the hierarchical combination, the dynamics of a three-inline configuration reduce to those of the single-tethered systems if the center spacecraft becomes exponentially stabilized by a simple independent control law. In other words, the above result shows that implementing an underactuated control law based on the single-tethered dynamics in Fig. 2 ensures the stability of the rotation rate and the relative motions in an inline three-spacecraft array (see the discussion in Ref. 5).

V. New Momentum Dumping Method for Saturated Wheels

If the linear velocity or angular velocity of each spacecraft is held constant, the increase of the tether length and external disturbance torque inevitably lead to the saturation of the wheel speed. For satellites in orbit, a pair of thrusters is conventionally used to dump the angular momentum of the saturated momentum

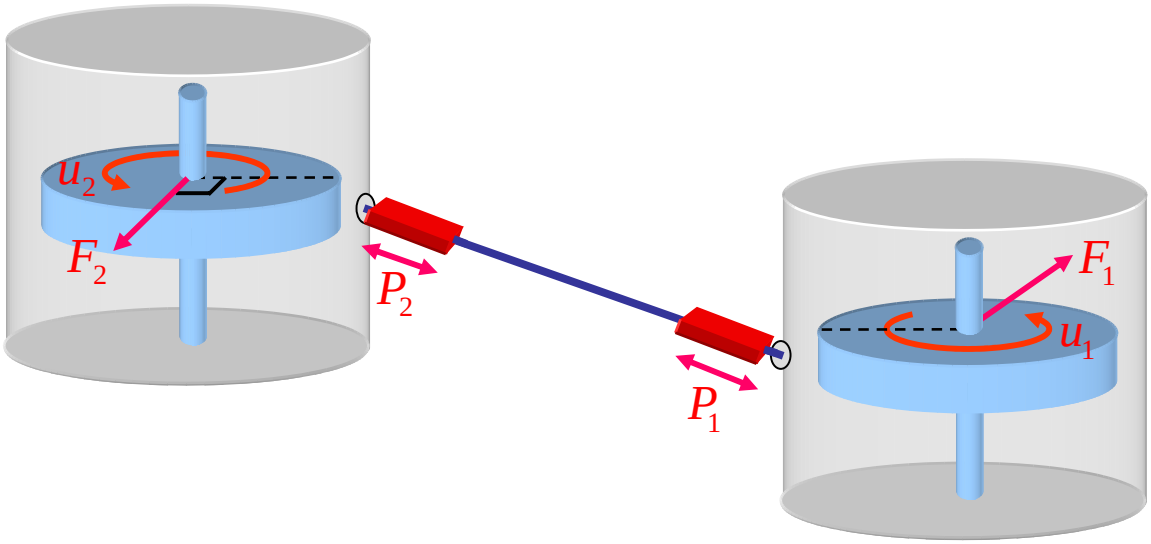

Figure 8. Two-spacecraft tethered system equipped with a high-bandwidth linear actuator on the tether (P), a reaction wheel (u), and a tangential thruster (F, not shown) in each spacecraft.

wheel. This section focuses on the issue associated with managing the saturated angular momentum once a tethered array spun by reaction wheels reaches its maximum size. A new technique that can be used to extend the array beyond this size is proposed. The proposed method maintains the desired array spin-rate and zero compound pendulum mode during the momentum dumping operation. Maintaining the zero compound pendulum mode without torque-generating thrusters poses a challenge since the reaction wheel, which directly controls the pendulum mode, is decelerated continuously in one direction.

Let us now assume that the tethered formation flight spacecraft shown in Fig. 8 are equipped with only a reaction wheel (u), a tangential force thruster (F), and a high-bandwidth translational actuator on the tether (P) in each spacecraft. The direction of F is perpendicular to the line between the tether attachment point and the CM of the spacecraft. It is shown that a planar rotating array of tethered spacecraft can control all relevant degrees of freedom using only one reaction wheel (u) in each spacecraft. Due to the Coriolis force exerted on the spacecraft, a radial motion of the tether can exert torque with respect to the compound pendulum mode ϕ in Fig. 8. Oscillatory motions of the tether from the force P can then be used as a means of controlling the pendulum mode. From the linearized dyanamics of Eq. (1), the dynamics of ϕ is coupled with $\dot{\ell}$ as

$$\ddot{\phi} + \frac{r\omega^2\big(I_r + m\ell(2r+\ell)\big)}{\ell I_G}\dot{\phi} = 2\frac{v}{\ell}\dot{\theta} + 2\frac{\omega}{\ell}\dot{\ell} - \frac{1}{m\ell}F + \frac{r+\ell}{I_G\ell}u \tag{45}$$

where v is the nominal tether speed, which is zero here.

Since $\dot{\ell}$ is mainly driven by the force P, we can control the compound pendulum mode ϕ by exerting the force P on the tether. Such an actuation method can be employed to dump the angular momentum stored on the reaction wheels. While constantly decelerating the wheel speed, the linear force P on the tether can be exerted in an oscillatory fashion to minimize the associated compound pendulum mode, while the linear thruster F maintains a constant array angular rate. In other words, it is straightforward to show that the system shown in Fig. 8 is fully controllable by F and P when u is not available (see Ref. 4). Hence, the momentum dumping method provides an alternative method for stabilizing the compound pendulum mode during momentum dumping operations.

A simulation of such a momentum dumping operation is presented in Fig. 9. The torque by reaction wheel (u) is set as $u = -0.01$ (Nm) such that the wheel speed can constantly be decelerated to zero. The tangential force thruster (F) and the translational actuator on the tether (P) exert the control forces in

order to maintain the same angular rate $\dot{\theta}$ and zero compound pendulum mode ($\phi, \dot{\phi} = 0$):

$$\begin{aligned} F &= -10\phi - 10\dot{\phi} - 10(\dot{\theta} - \dot{\theta}_d) \\ u &= -0.01 \\ P &= -10\phi - 10\dot{\phi} - 10(\dot{\theta} - \dot{\theta}_d) - 40(\ell - \ell_d) - 40\dot{\ell} \end{aligned} \tag{46}$$

The top plot of Fig. 9(a) shows the change in the angular momentum of the reaction wheel due to the constant deceleration $u = -0.01$ (Nm) while the control forces F and P effectively maintain the control states at the reference points (bottom plot). Figure 9(b) shows that the usage of the linear thruster (F) to maintain the array angular rate is relatively small. In contrast, large P is required to stabilize the compound pendulum mode in the absence of the RWA torque u. Small oscillations of both the control states and the tether length are acceptable since no interferometric observation is scheduled during the momentum dumping operation.

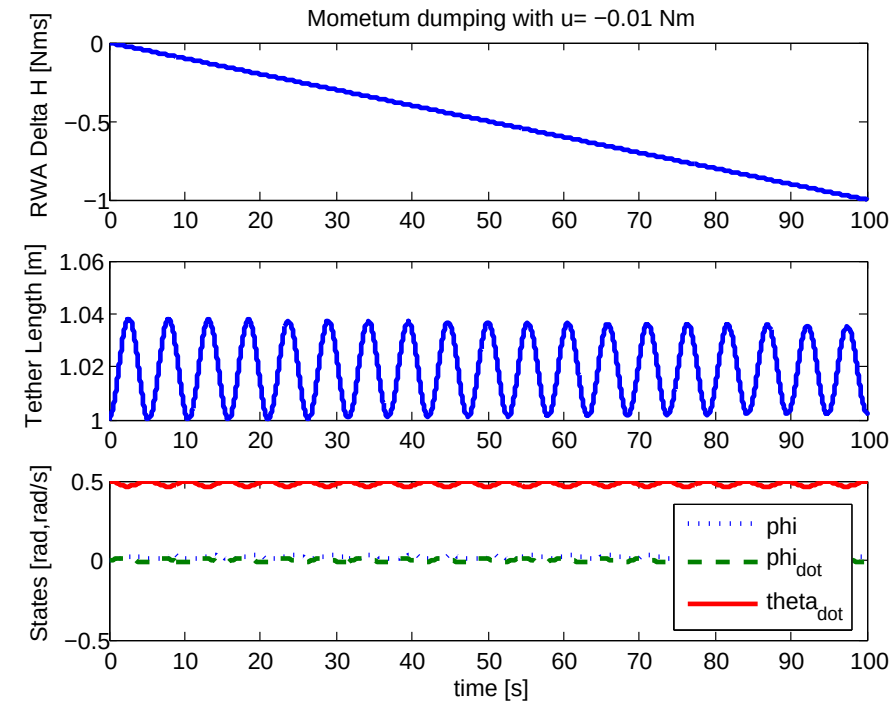

(a) Change in the RWA angular momentum and the control states

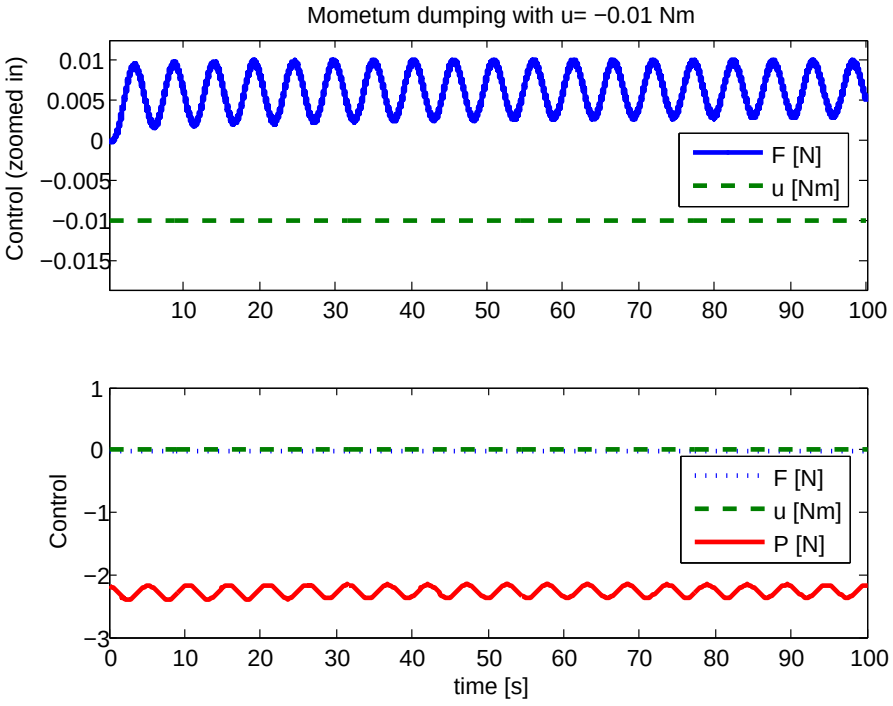

(b) Control

Figure 9. Momentum dumping operation with stabilization

VI. Control Simulation Results

We illustrate that the nonlinear control approach is superior to the linear control in tracking a time-varying trajectory. The desired angular rate of the array $\dot{\theta}_d$ is given as

$$\dot{\theta}_d = 0.25 + 0.02e^{-\tau t}(1 - \cos(2\pi f t)) \tag{47}$$
$$\ddot{\theta}_d = 0.02e^{-\tau t}[2\pi f(\sin(2\pi f t)) - \tau(1 - \cos(2\pi f t))]$$

where f=0.01, τ=0.02. The control law is also required to minimize the compound pendulum modes such that $\phi_d, \dot{\phi}_d = 0$ while trying to follow $\dot{\theta}_d$.

The initial conditions are defined as $\dot{\theta}_0$=0.25 rad/s, $\phi_0 = 0.1$ rad, and $\dot{\phi}_0 = -0.05$ rad/s. The physical parameters used in the simulations are selected from the actual values of the SPHERES testbed on the new air-bearing carriage.[4] The radius of SPHERES, r is 0.15 m, the mass of SPHERES with the air-bearing carriage, m is 20.346 kg, and the moment of inertia I is 0.178 kgm^2. The tether length ℓ is either 0.5 m or 1 m.

Figure 10 shows the performance of the nonlinear tracking control using the feedback linearization of the reduced variables in Eq. (28). The gains are defined as $K = 1$ and $D = 2$. The nonlinear control is denoted by NLFL and compared with the LQR control. For the LQR control, the Q weighting matrix is diag($\begin{bmatrix}1 & 5 & 1\end{bmatrix}$) and the nominal angular rate of $\dot{\theta} = \omega$=0.25 rad/s are used. The simulation clearly indicates that the nonlinear control is superior to the LQR control in terms of tracking error. Both control approaches turn out to be equally efficient in minimizing the compound pendulum mode ($\phi, \dot{\phi}$). As the tether length ℓ increases from 0.5 m (Fig. 10(a)) to 1.0 m (Fig. 10(b)), the tracking performance for the LQR control degrades even though the change in the tether length was taken into account in computing the optimal LQR gains. This degradation in the performance of the LQR control has to do with the fact that the underactuated tethered system becomes less controllable as the tether length increases (see Fig. 4). In contrast, the nonlinear control achieves the same level of performance regardless of the tether length variation. In addition, cumbersome gain-scheduling is not required for the nonlinear control approach.

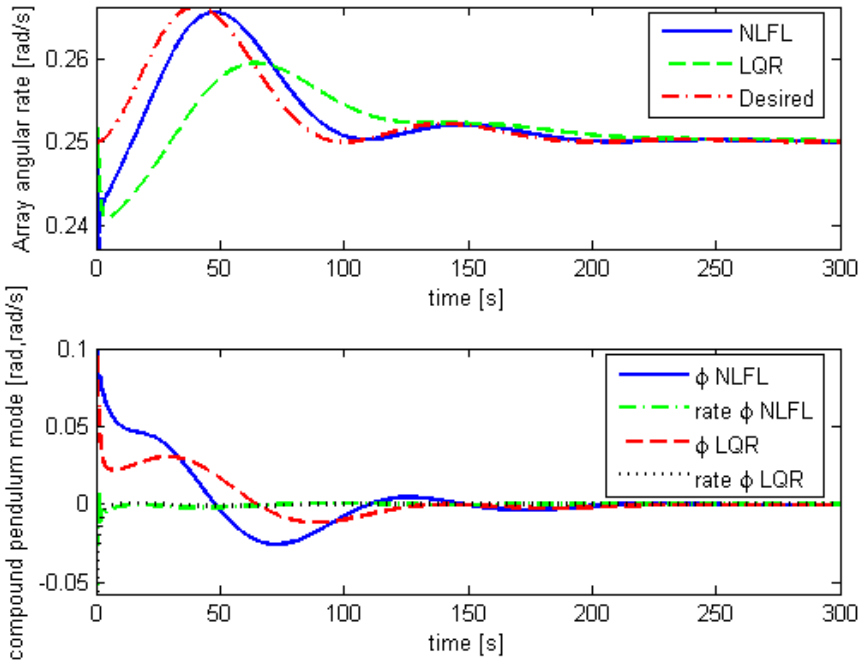

(a) tether length=0.5 m

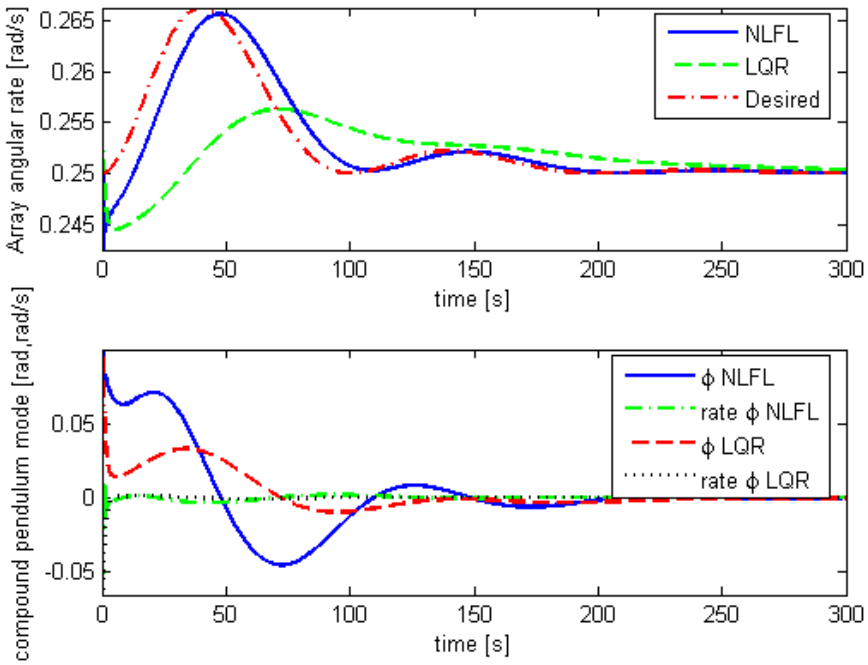

(b) tether length=1.0 m

Figure 10. Nonlinear tracking control using the feedback linearization of the reduced variable (NLFL) in Section IV-A and the LQR control

VII. Experimental Validation using SPHERES

Our approach to reduce the complexity of controlling multiple spacecraft connected by tethers is decentralization by oscillation synchronization.[5] We successfully performed all of our underactuated control tests using this decentralization technique. In this manner, we were able to dramatically increase the control bandwidth and reliability by eliminating the need for inter-satellite communications. We present key closed-loop control results.

A. Overview of SPHERES Satellite

The SPHERES testbed was developed as part of the ongoing research initiatives of the MIT-SSL that utilize the space environment provided by the International Space Station (ISS) to validate dynamics and control algorithms of distributed spacecraft control, estimation, and autonomy. At the time of writing, several SPHERES nano-satellites were launched to the ISS for control experiments in a three-dimensional environment. Motivated by the successful experimental results in this thesis, tethered formation flying experiments at ISS are currently being pursued. The zero-gravity facility at ISS will provide six degrees-of-freedom (DOF) for each satellite to fully test control and estimation algorithms for NASA's future stellar interferometer missions such as TPF and SPECS.[9] In the mean time, we verify our algorithms in a less risky and more cost-effective environment including NASA's KC-135 reduced-gravity facility and the 2-dimensional flat floor facilities at MIT and NASA MSFC. The three main operational environments of the SPHERES testbed are presented in Figure 11. The top two pictures show the zero-gravity 6 DOF environment in the ISS (top left) and NASA's KC-135 flight (top right). The bottom pictures depict SPHERES sitting on the air-bearing carriages at the MSFC flat floor, which provides three DOF: yaw rotation and x,y translations. The individual self-contained satellites have the ability to maneuver in up to six Degrees of Freedom (DOF) (three rotations and three translations), to communicate with each other and with the laptop control station, and to identify their position and attitude with respect to each other and to the experiment global reference frame. The detailed description on SPHERES can be found in Ref. 4.

B. Decentralized Gain-Scheduled LQR Control

Figures 12 and 13 show the experimental data of a spin-up and deployment maneuver on the NASA MSFC flat floor, using two tethered SPHERES controlled using decentralized control laws. Still pictures from the video of the same test are presented in Fig. 14. Such a maneuver emulates a possible mission scenario in which a completely docked, tethered-spacecraft array is deployed from a mother spacecraft. All the data was transmitted to the laptop computer at the frequency of 10 Hz in realtime via the wireless RF communication. It should also be noted that all the state estimates are delivered from the Kalman filter, which incorporates both the F/T sensor measurements and the angular rates from the gyroscope.[4]

The controller implemented in this test was a decentralized gain-scheduled LQR controller running at 100 Hz. The scheduled LQR gain is a continuous function of $\dot{\theta}$ but a discrete function of ℓ. This controller is significant in its own right, since it validates the feasibility of the minimal fuel control approach by controlling all the relevant degrees of freedom, including the array spin rate, using only the reaction wheels.

The top plot of Figures 12 and 13 shows the actual array angular rate ($\dot{\theta}$) as it is commanded to follow a desired trajectory ($\dot{\theta}_{ref}$). For SPHERE #1, the RMS of the error between $\dot{\theta}$ and $\dot{\theta}_{ref}$ after the initial spin-up (t$\geq$44.8 sec) is 0.04 rad/s, ignoring the transient period (t=75-86 sec), which occurred due to the abrupt movement of the tether motor at 75 seconds. Such an undesirable response arises due to two problems: the initial stiction of the tether motor and the occasional tangling of the tether on the motor spool. These issues will be resolved in the new flight version described in Ref. 4. Nevertheless, the tracking error remained effectively well within $\pm$ 0.03 rad/s (1.7 deg/s) at the steady-state. During the period of t=100-112 sec, both the satellites were spinning on a particularly rough portion of the floor, thereby degrading the tracking performance.

While tracking the desired trajectory, the controller minimizes the compound pendulum motions ($\phi, \dot{\phi}$), shown in the middle plot of each figure. The ϕ and $\dot{\phi}$ before 75 sec should be discarded since the two SPHERES were docked, thereby preventing compound pendulum motion. The estimated tether length (ℓ) in the bottom plot indicates that the two SPHERES were completely docked when they started from rest ($\dot{\theta} = 0$) at 34 seconds. The estimated tether length was computed off-line from the On/Off time-history of

(a) Formation flying experiments at ISS

(b) Formation flying experiments onboard KC-135 flight

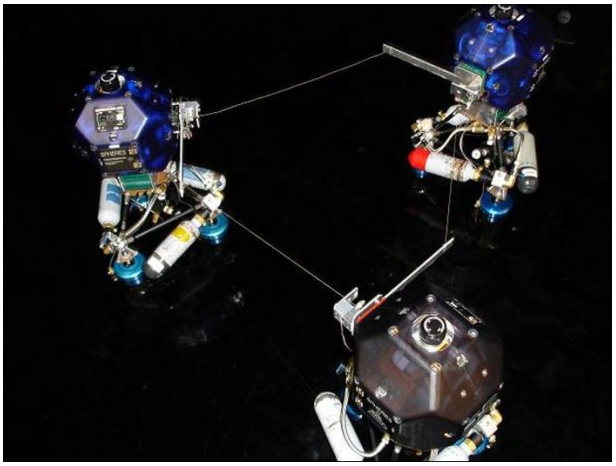

(c) Three triangular configuration on MSFC flat floor

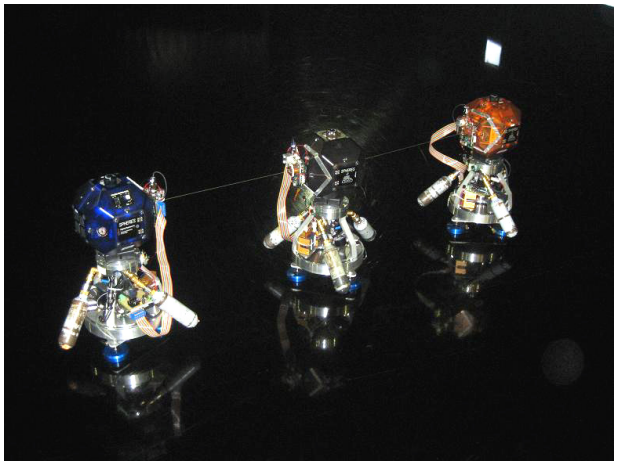

(d) Three inline configuration on MSFC flat floor

Figure 11. Three operational environments of SPHERES. ISS (a), KC 135 reduced-gravity flight (b), NASA MSFC flat floor (c,d) left and right)

the tether motor, since range measurements from the U/S system were not available in realtime due to the blocked IR transmission.

The RMS errors of the compound pendulum mode, ignoring the rough period (t=75-86 sec) are found to be smaller than 0.03 rad/s (1.7 deg/s). In particular, the bearing angle $\dot{\phi}$ for SPHERE #1 remained within $\pm$ 0.03 rad/s (1.7 deg/s) for 91% of the time span while the ϕ measurement failed for some unknown reason. The particular LQR controller implemented in this test had a zero ϕ gain, thereby minimizing the effect of such a sensor failure. For SPHERE #2, ϕ remained within the bound of $\pm$ 0.03 rad for 90% of time, while $\dot{\phi}$ remained within $\pm$ 0.03 rad/s for 91.3% of time.

VIII. Conclusion

We proposed a novel approach for controlling the array spin rate and relative attitude without thrusters by exploiting the coupled dynamics. Such a tethered system without thrusters is underactuated since it has fewer inputs than configuration variables. This work reports the first propellant-free underactuated control results for tethered formation flying spacecraft. Such an underactuated control approach is particularly beneficial to stellar interferometers due to the increased mission life span and reduced optical contamination by exhaust from the thrusters. This article also fulfilled the potential of the proposed underactuated strategy by providing a new momentum dumping method that does not use torque-generating thrusters. Furthermore, using the gain-scheduled LQR control law implemented in the SPHERES testbed, we successfully demonstrated that a planar rotating array of tethered spacecraft could control all relevant degrees of freedom using

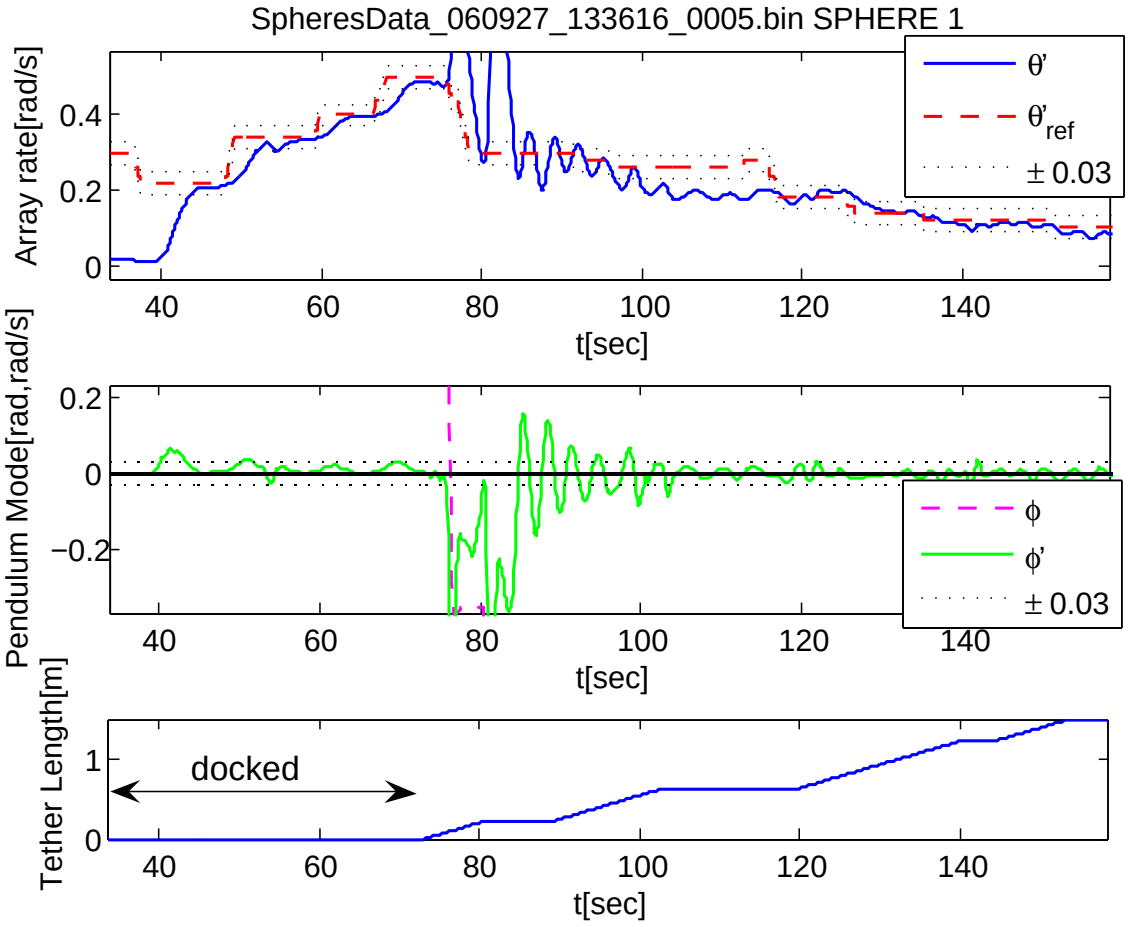

Figure 12. State estimates and commands from SPHERE #1 during spin-up and deployment of the two-satellite tethered formation using gain-scheduled LQR

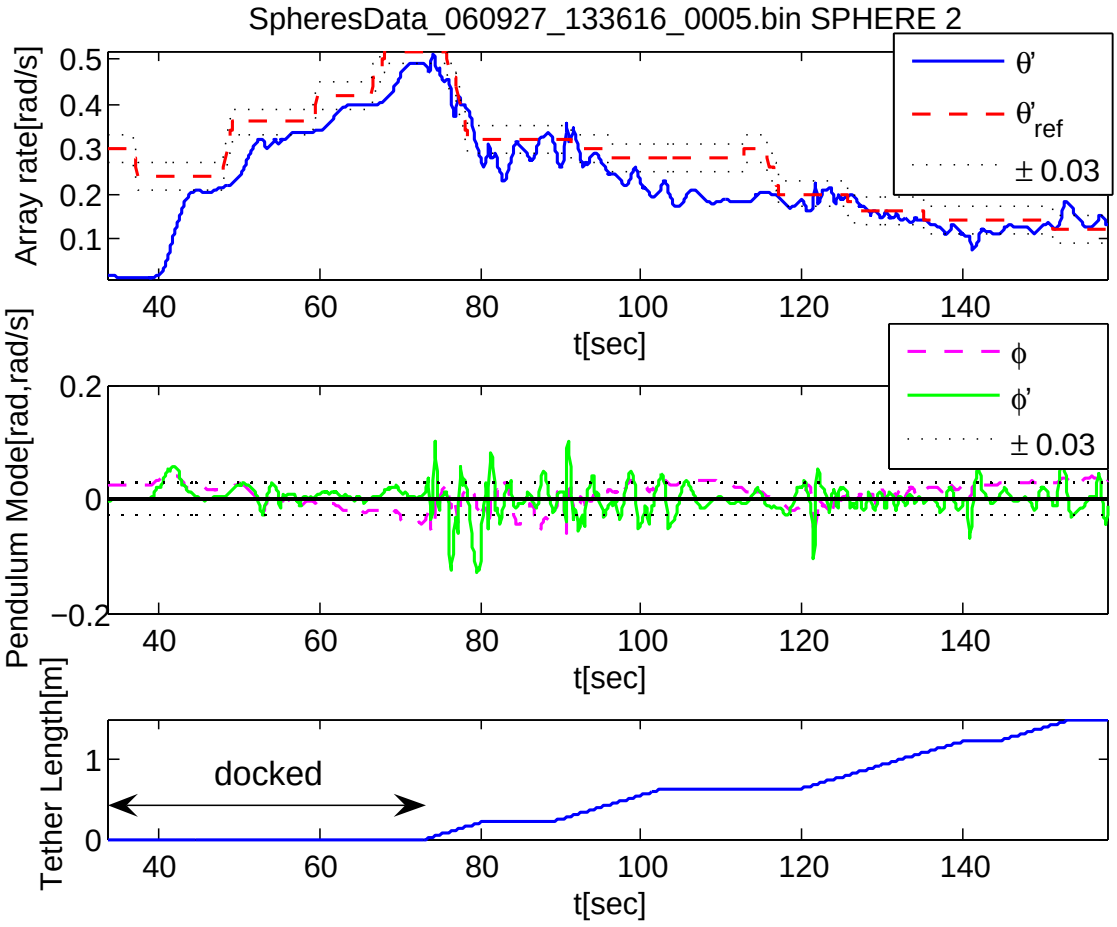

Figure 13. State estimates and commands from SPHERE #2 during spin-up and deployment of the two-satellite tethered formation using gain-scheduled LQR

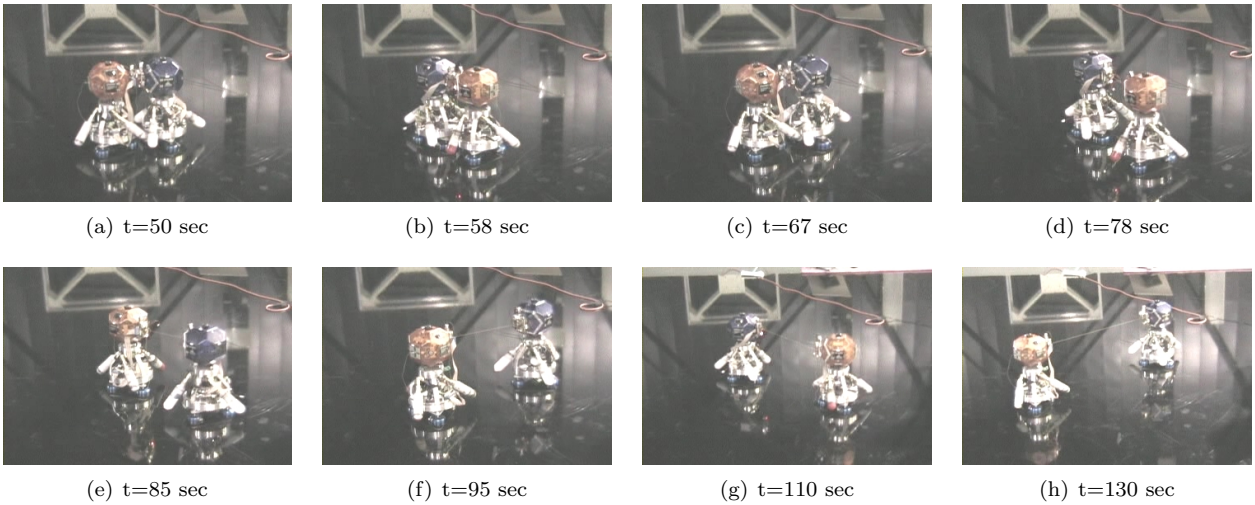

(a) t=50 sec (b) t=58 sec (c) t=67 sec (d) t=78 sec

(e) t=85 sec (f) t=95 sec (g) t=110 sec (h) t=130 sec

Figure 14. Two-SPHERES spin-up maneuver

only one reaction wheel in each spacecraft.

In contrast with linear systems, in which an underactuated control law can be synthesized easily, designing a nonlinear controller for nonlinear underactuated systems is a difficult control problem, mainly due to the lack of full state feedback linearizability. In this paper, we derived several control laws for spinning tethered systems: gain-scheduled LQR control, feedback linearization via momentum decoupling, and backstepping. Our simulation results indicate that the nonlinear control methods are much more efficient in tracking time-varying trajectories than LQR control.

For future work, developing a robust nonlinear underactuated control method that deals with model uncertainties and sensor noise would be an interesting and challenging research topic. Even though the modeling on the two-dimensional rotational plane is justified by the decoupling, it would also be useful to extend such an underactuated control strategy to three-dimensional attitude dynamics. In particular, precessing the array rotation might also be achievable using underactuated tethered systems.

Acknowledgments

The authors would like to gratefully acknowledge the NASA Goddard Space Flight Center (Contract Monitor Dr. David Leisawitz) for both financial and technical support for the MIT-SSL and Payload Systems (PSI) SPHERES Tether program. The authors also thank the MIT SPHERES team including Danielle Adams, Alvar Saenz-Otero and Christophe Mandy for the technical discussions and support.

References

[1]Bloch, A.M, Baillieul, J., Crouch, P., and Marsden, J., *Nonholonomic Mechanics and Control*, Springer-Verlag, New York, 2003.

[2]Brown, S.C., Passino, K.M., "Intelligent Control for an Acrobot," Journal of Intelligent and Robotic Systems, Vol. 18, pp. 209-248, 1997.

[3]Bullo, F., and Lewis, A.D., *Geometric Control of Mechanical Systems- Modeling Analysis, and Design for Simple Mechanical Control Systems*, Texts in Applied Mathematics, Springer-Verlag, 2004.

[4]Chung, S.-J., *Nonlinear Control and Synchronization of Multiple Lagrangian Systems with Application to Tethered Formation Flight Spacecraft*, Ph.D. Thesis, MIT, 2007.

[5]Chung, S.-J., Slotine, J.-J.E., Miller, D.W., "Nonlinear Model Reduction and Decentralized Control of Tethered Formation Flight," to appear in Journal of Guidance, Control, and Dynamics, 2007.

[6]Frazzoli, Emilio, *Robust Hybrid Control for Autonomous Vehicle Motion Planning*, Ph.D. Thesis, Department of Aeronautics and Astronautics, MIT, May 2001.

[7]Harwit, M. "Kilometer-Baseline Far-Infrared/Submillimeter Interferometer Vision Mission: Final Report," Interferometer Vision Mission Team. May, 2005.

[8]Krstic, K., Kanellakopoulos, I., and Kokotovic, P., *Nonlinear and Adaptive Control Design*, John Wiley and Sons, 1995.

[9]Leisawitz, D., et al., "Scientific Motivation and Technology Requirements for the SPIRIT and SPECS Far-infrared/Submillimeter Space Interferometers," Proceedings SPIE 4013, 2000, p. 36.

[10]Lohmiller, W., and Slotine, J.J.E., "On Contraction Analysis for Nonlinear Systems," Automatica, 34(6), 1998.

[11]Lorenzini, E., Harwit, M., Bombardelli, C., Miller, D., Farley, R., Leisawitz, D., Rinehart, S., "The Role of Tethers in Far-Infrared/Submillimeter Astronomical Interferometry from Space," Astrophys Space Sci., 302:225-239, 2006.

[12]Murray, R.M. and Hauser, J., "A Case Study in Approximate Linearization: The Acrobot Example," University of California, Berkeley Technical Report No. UCB/ERL M91/46, 1991.

[13]Olfati-Saber, R., *Nonlinear Control of Underactuated Mechanical Systems with Application to Robotics and Aerospace Vehicles*, Ph.D. thesis, Department of EECS, MIT, February 2001.

[14]Reyhanoglu, M., van der Schaft, A., McClamroch, N. H., and Kolmanovsky, I., "Dynamics and Control of a Class of Underactuated Mechanical Systems," IEEE Transactions on Automatic Control, 44(9):1663-1671, 1999.

[15]Rugh, W.J., and Shamma, J.S., "Research on Gain Scheduling," Automatica, 36, 1401-1425, 2000.

[16]Slotine, J.-J.E., and Li, W., *Applied Nonlinear Control*, Prentice Hall,. New Jersey, 1991.

[17]Spong, M.W., "Swing Up Control Problem For the Acrobot," IEEE Control Systems Magazine, Feb., 1995.

[18]Tedrake, R. L., *Applied Optimal Control for Dynamically Stable Legged Locomotion*, Ph.D. thesis, Massachusetts Institute of Technology, 2004.

[19]Tsiotras, P., Corless, M., and Longuski, J.M, "A Novel Approach to the Attitude Control of Axi-Symmetric Spacecraft," Automatica, Vol. 31, No. 8, pp. 1099-1112, 1995.

[20]Tsiotras, P., and Luo, J., "Reduced-Effort Control Laws for Underactuated Rigid Spacecraft," AIAA Journal of Guidance, Control, and Dynamics, Vol. 20, No. 6, pp. 1089–1095, 1997.

[21]Tsiotras, P. and Luo, J., "Control of Underactuated Spacecraft with Bounded Inputs," Automatica, Vol. 36, No. 8, pp. 1153-1169, 2000.

[22]Vidyasagar, M., *Nonlinear Systems Analysis*, 2nd ed., SIAM Classics in Mathematics, SIAM, Philadelphia, 1993.

[23]Wang, W., Yi, J., Zhao, D., and Liu, D., "Design of a Stable Sliding-Mode Controller for a Class of Second-Order Underactuated Systems," IEE Proc.-Control Theory Appl., Vol. 151, No. 6, November 2004.

[24]Woolsey, C., Reddy, C.K., Bloch, A.M., Chang, D.E., Leonard, N.E., and Marsden, J.E., "Controlled Lagrangian systems with gyroscopic forcing and dissipation," European Journal of Control (Special Issue on Lagrangian and Hamiltonian Methods for Nonlinear Control) 10(5), pp. 478-496, December 2004.

[25]Zhang, M., and Tarn, T.-J., "A Hybrid Switching Control Strategy for Nonlinear and Underactuated Mechanical Systems," IEEE Trans. on Automatic Control, Vol. 48, No. 10, October 2003.